



Remote sensing of
different absorbing
aerosol species

G. L. Schuster et al.

This discussion paper is/has been under review for the journal Atmospheric Chemistry and Physics (ACP). Please refer to the corresponding final paper in ACP if available.

Remote sensing of soot carbon – Part 1: Distinguishing different absorbing aerosol species

G. L. Schuster¹, O. Dubovik², and A. Arola³

¹NASA Langley Research Center, Hampton, VA, USA

²Laboratoire d'Optique Atmosphérique, Université de Lille-1, CNRS, Villeneuve d'Ascq, France

³Finnish Meteorological Institute, Kuopio, Finland

Received: 24 March 2015 – Accepted: 20 April 2015 – Published: 12 May 2015

Correspondence to: G. L. Schuster (gregory.l.schuster@nasa.gov)

Published by Copernicus Publications on behalf of the European Geosciences Union.

Title Page

Abstract

Introduction

Conclusions

References

Tables

Figures



Back

Close

Full Screen / Esc

Printer-friendly Version

Interactive Discussion



Abstract

We describe a method of using the aerosol robotic network (AERONET) size distributions and complex refractive indices to retrieve the relative proportion of carbonaceous aerosols and iron oxide minerals. We assume that soot carbon has a spectrally flat refractive index, and that enhanced imaginary indices at the 440 nm wavelength are caused by brown carbon or hematite. Carbonaceous aerosols can be separated from dust in imaginary refractive index space because 95 % of biomass burning aerosols have imaginary indices greater than 0.0042 at the 675–1020 nm wavelengths, and 95 % of dust has imaginary refractive indices of less than 0.0042 at those wavelengths. However, mixtures of these two types of particles can not be unambiguously partitioned on the basis of optical properties alone, so we also separate these particles by size. Regional and seasonal results are consistent with expectations. Monthly climatologies of fine mode soot carbon are less than 1.0 % by volume for West Africa and the Middle East, but the southern Africa and South America biomass burning sites have peak values of 3.0 and 1.7 %. Monthly-averaged fine mode brown carbon volume fractions have a peak value of 5.8 % for West Africa, 2.1 % for the Middle East, 3.7 % for southern Africa, and 5.7 % for South America. Monthly climatologies of iron oxide volume fractions show little seasonal variability, and range from about 1.1 to 1.7 % for coarse mode aerosols in all four study regions. Finally, our sensitivity study indicates that the soot carbon retrieval is not sensitive to the component refractive indices or densities assumed for carbonaceous and iron oxide aerosols, and differs by only 15.4 % when these parameters are altered from our chosen baseline values. The associated soot carbon absorption aerosol optical depth (AAOD) does not vary at all when these parameters are altered, however, because the retrieval is constrained by the AERONET optical properties.

Remote sensing of different absorbing aerosol species

G. L. Schuster et al.

Title Page

Abstract

Introduction

Conclusions

References

Tables

Figures



Back

Close

Full Screen / Esc

Printer-friendly Version

Interactive Discussion



1 Introduction

Soot carbon (sC) is a byproduct of combustion that is composed of aggregated graphite spheres (Andreae and Gelencsér, 2006). It is often called light absorbing carbon (LAC), black carbon (BC), refractory black carbon (rBC), or elemental carbon (EC) in the scientific literature (depending upon the measurement technique), but we prefer the carbonaceous aerosol definitions nicely presented by Andreae and Gelencsér (2006). Thus, the term “soot carbon” presented here is equivalent to “light absorbing carbon” in Bond and Bergstrom (2006) and “black carbon” or “refractory black carbon” in Bond et al. (2013). We use the term brown carbon (BrC) for absorbing organic matter to distinguish these species from organic compounds that do not absorb significantly at visible wavelengths (Jacobson, 1999; Kirchstetter et al., 2004; Kanakidou et al., 2005; Hoffer et al., 2006; Schnaiter et al., 2006; Sun et al., 2007; Dinar et al., 2008; Chen and Bond, 2010). Our BrC is equivalent to OM in Chung et al. (2012).

Atmospheric warming caused by sC is highly uncertain. The most recent Intergovernmental Panel on Climate Change (IPCC; Boucher et al., 2013) estimate of the sC direct radiative forcing for fossil fuel and biofuel sC is $+0.4 \text{ W m}^{-2}$ (with an uncertainty range of $+0.05$ to $+0.8 \text{ W m}^{-2}$); this estimate is based upon the AeroCom Phase II model simulations of Myhre et al. (2013a) and the scaled absorption aerosol optical depth (AAOD) findings of Bond et al. (2013). The direct effect does not capture all forcing mechanisms, however, and Bond et al. (2013) estimate that the industrial-era climate forcing associated with sC is $\text{RF}_{\text{sC}} = +1.1 \text{ W m}^{-2}$, with an uncertainty range of $+0.17$ to $+2.1 \text{ W m}^{-2}$ when all forcing mechanisms are included. Soot carbon radiative forcing is 2nd only to CO_2 radiative forcing as a contributor to global warming (Ramanathan and Carmichael, 2008; Bond et al., 2013). Finally, although CO_2 radiative forcing is larger than sC radiative forcing ($\text{RF}_{\text{CO}_2} = 1.8 \pm 0.19 \text{ W m}^{-2}$, per Myhre et al., 2013b), the range of uncertainty for sC forcing is much larger than the range of uncertainty for CO_2 forcing.

Remote sensing of different absorbing aerosol species

G. L. Schuster et al.

Title Page

Abstract

Introduction

Conclusions

References

Tables

Figures



Back

Close

Full Screen / Esc

Printer-friendly Version

Interactive Discussion



The cooling associated with all aerosols in the IPCC 5th assessment report is $-0.35 \pm 0.5 \text{ W m}^{-2}$; thus, soot carbon warming from the direct effect alone reduces aerosol cooling by about 53 %, which has prompted suggestions that reducing sC could be a viable method of mitigating global warming in the short term (Jacobson, 2010).

Others have noted that non-absorbing aerosols that are co-emitted with sC make this difficult in practice (Bond et al., 2013).

sC warming is uncertain because modeled sC concentrations and the associated absorption are unconstrained by in situ measurements. The difficulty is the lack of available sC data. The Interagency Monitoring of Protected Visual Environments (IMPROVE) network provides routine elemental carbon (EC) measurements at the surface in the United States, but mainly in remote areas (Malm et al., 1994). Some surface measurements are also available in other parts of the world (Koch et al., 2009), but global coverage of sC concentration and absorption is not available from satellite data.

Modeled sC concentrations are too high by a factor of 1.6 on average over North America when compared to long term in situ measurements at the surface (Park et al., 2003; Koch et al., 2009), and too high by a factor of 5 to 7.9 when compared to aircraft measurements during field campaigns over the United States, Canada, and the Pacific Ocean (Koch et al., 2009; Schwarz et al., 2010). Modeled AAOD, on the other hand, is lower than the aerosol robotic network (AERONET) and ozone monitoring instrument (OMI) products by a factor of 0.69 and 0.85 over North America (Koch et al., 2009), and a factor of 2–4 lower than AERONET worldwide (Sato et al., 2003). Thus, the link between sC emissions, sC concentrations, and AAOD is not straightforward, and the low bias in modeled AAOD over North American source regions can not be simply associated with errors in the sC emission inventories alone.

One problem is that sC is not the only absorbing aerosol in the atmosphere, as BrC and iron oxides in dust are significant absorbers at ultraviolet through mid-visible wavelengths (Kerker et al., 1979; Chen and Cahan, 1981; Hsu and Matijević, 1985; Gillespie and Lindberg, 1992; Bedidi and Cervelle, 1993; Kirchstetter et al., 2004; Sun et al., 2007; Derimian et al., 2008; Chen and Bond, 2010). Separating the absorption

associated with sC from the absorption associated with these other aerosols is not trivial; this is especially true for absorption at the 550 nm wavelength favored by many studies, since all of these aerosol species absorb at that wavelength.

Thus, there is a need for determining the relative proportions of sC, BrC, and iron oxide in atmospheric aerosols. AERONET provides aerosol size distributions and complex refractive index at four wavelengths (440, 675, 870, and 1020 nm) at hundreds of surface sites throughout the world (Holben et al., 1998, 2001; Dubovik and King, 2000; Dubovik et al., 2000). This information can be used to retrieve the relative proportions of carbonaceous aerosols and iron oxide minerals. Schuster et al. (2005) retrieved sC from the aerosol complex refractive index provided in the AERONET database by assuming that all aerosol absorption is associated with sC. Arola et al. (2011) used the spectral variability of the imaginary refractive index in the AERONET database to retrieve BrC. Similarly, Li et al. (2013) used AERONET complex refractive indices to retrieve sC, BrC, and dust over Beijing. Wang et al. (2013) added single-scatter albedo (SSA) as an additional constraint to these refractive index approaches. Koven and Fung (2006) used the spectral variability of the imaginary index to retrieve hematite concentrations at dust sites. Other methods of retrieving sC from AERONET data include the absorption Angstrom exponent (AAE) approach (Chung et al., 2012; Bahadur et al., 2012) and the Bond et al. (2013) approach. However, these last two approaches assume that all absorbing aerosols are externally mixed (which is inconsistent with the AERONET retrieval algorithm), and do not necessarily maintain a link to the measured radiances (as discussed in Sect. 5 and Schuster et al., 2015).

Knowledge of both sC mixing ratios and AAOD are important for constraining how sC is transported, removed, and mixed with other aerosols in the global models. Here, we present a method of deriving column concentrations of sC mass and mixing ratios that are consistent with the AERONET AAODs, size distributions, and refractive indices. The method is an improvement over previous methods because it uses different mixtures of aerosol species for the fine mode than for the coarse mode. That is, we as-

Remote sensing of different absorbing aerosol species

G. L. Schuster et al.

Title Page

Abstract

Introduction

Conclusions

References

Tables

Figures



Back

Close

Full Screen / Esc

Printer-friendly Version

Interactive Discussion



sume that the fine mode is dominated by carbonaceous absorbing aerosols, and that the coarse mode is dominated by the iron oxides commonly found in mineral aerosols.

2 Method

There are four absorbing aerosols species that are commonly found in the atmosphere: soot carbon (sC), brown carbon (BrC), hematite, and goethite. Soot carbon and brown carbon are produced by the same combustion sources, and generally coexist in aerosol layers. Hematite and goethite are iron oxides that are different forms of “free” iron, and typically appear together as well (Arimoto et al., 2002; Lafon et al., 2006; Shi et al., 2012; Formenti et al., 2014). Our task is to separate the various contributions of these absorbing aerosol species.

Our approach utilizes imaginary refractive index, which we present for the common absorbing aerosols in Fig. 1. Note that the BrC imaginary refractive index is substantial at UV wavelengths, decreases dramatically as wavelength increases throughout the visible, and absorbs negligibly at wavelengths longer than about 0.700 μm (Kirchstetter et al., 2004; Hoffer et al., 2006; Sun et al., 2007; Dinar et al., 2008; Chakrabarty et al., 2010; Chen and Bond, 2010; Lack et al., 2012).

Dust particles containing hematite also have a strong spectral signature, with the greatest absorption occurring at the UV and blue wavelengths. It is generally assumed that hematite is spectrally flat in the near infrared region ($\sim 0.700\text{--}1.0\ \mu\text{m}$), but measurements are sparse at those wavelengths. Nonetheless, the AERONET climatologies shown in Fig. 1 corroborate a flat spectral signature at the 0.67–1.02 μm wavelengths for absorbing dust, as does Dubovik et al. (2002); Kim et al. (2011); and Wagner et al. (2012).

Since both BrC and hematite have strong spectral dependence for the imaginary index, mixtures of carbonaceous aerosols and dust can not be unambiguously partitioned on the basis of the imaginary index alone. Fortunately, we can separate these particles by size, since carbonaceous particles are dominated by fine mode particles

Remote sensing of different absorbing aerosol species

G. L. Schuster et al.

Title Page

Abstract

Introduction

Conclusions

References

Tables

Figures



Back

Close

Full Screen / Esc

Printer-friendly Version

Interactive Discussion



Remote sensing of different absorbing aerosol species

G. L. Schuster et al.

Title Page

Abstract

Introduction

Conclusions

References

Tables

Figures



Back

Close

Full Screen / Esc

Printer-friendly Version

Interactive Discussion



and dust is dominated by coarse mode particles; thus, the retrieval initially populates the fine mode with BrC and the coarse mode with dust. Unfortunately, the AERONET imaginary indices over regions like west Africa often indicate greater spectral dependencies than is observed in biomass burning aerosols (requiring BrC/sC mass ratios greater than 15.2 in the fine mode). Likewise, the 675–1020 nm imaginary indices in the AERONET database are often greater than is observed in pure dust, and would require free iron fractions greater than 10% in the coarse mode (if no other absorbers were present). We solve this difficulty by populating some of the fine mode with iron oxide and some of the coarse mode with carbonaceous aerosols (which is consistent with what is found in nature).

The foundation of the retrieval is presented in Sect. 2.1, which demonstrates the range of imaginary refractive indices that we can reasonably expect to observe for dust or carbonaceous aerosols. Next, we use AERONET data to illustrate how the imaginary refractive indices of dust and carbonaceous aerosols differ (Sect. 2.2). Finally, the results of Sects. 2.1 and 2.2 are applied in Sect. 2.3 to retrieve the component volume fractions of sC, BrC, and free iron.

2.1 Aerosol layers with two absorbing species

If we know that we are observing “pure” dust or “pure” biomass burning aerosols, we can use the imaginary refractive indices shown in Fig. 1 to retrieve the relative fractions of hematite and goethite in the dust, or sC and BrC in the biomass burning aerosols. Later, we will discuss a technique for retrieving absorbing aerosol species in more complex aerosol mixtures. The basic procedure is presented in Schuster et al. (2005), which we briefly review here.

A schematic of our approach is illustrated in Fig. 2. The operational AERONET product assumes that all particles have the same refractive index, which implies that all particles are internally mixed. Thus, our task is to determine an internal mixture of aerosols that produce the AERONET refractive indices at all available wavelengths. The complex refractive index of an aerosol mixture that contains a non-absorbing host aerosol

and two absorbing inclusions can be expressed as a function (F) of the volume fraction of the inclusions (f_i), the complex refractive index of the inclusions ($m_i = n_i + ik_i$), and the complex refractive index of the host aerosol (m_{host}):

$$m_{\text{mix}}(\lambda_j) = F(f_1, f_2, m_1(\lambda_j), m_2(\lambda_j), m_{\text{host}}(\lambda_j)), \quad (1)$$

where λ_j represents wavelength of interest. In practice, Eq. (1) is implemented using the Maxwell Garnett effective medium approximation (EMA), the Bruggeman EMA, or volume averaging (Bohren and Huffman, 1983; Schuster et al., 2005). Volume averaging provides the simplest method for determining m_{mix} (i.e., $m_{\text{mix}} = \sum_i f_i m_i$), but the Maxwell Garnett and Bruggeman EMAs are determined from the complex dielectric constants of the host and inclusions, and therefore require additional equations for conversion to the refractive index (see Bohren and Huffman, 1983). The Maxwell Garnett and Bruggeman EMAs differ by less than 5% (Lesins et al., 2002), so we use the Maxwell Garnett EMA because of its superior computational speed.

If the inclusion refractive indices (m_i) are known, we can compute the inclusion fractions and the host refractive index that “best” matches the AERONET refractive indices (m_{rtr}) by iterating f_i and n_{host} until a minimum χ^2 value is achieved (Schuster et al., 2005):

$$\chi^2 = \sum_{j=1}^4 \frac{(n_{\text{rtr}}(\lambda_j) - n_{\text{mix}}(\lambda_j))^2}{n_{\text{rtr}}(\lambda_j)} + \frac{(k_{\text{rtr}}(\lambda_j) - k_{\text{mix}}(\lambda_j))^2}{k_{\text{rtr}}(\lambda_j)} \rightarrow 0, \quad (2)$$

The solution is unique because the co-emitted absorbing aerosols that we consider (sC and BrC or hematite and goethite) have different spectral signatures, as shown in Fig. 1. Thus, the sC mixing ratio in the fine mode is determined by the 670–1020 nm wavelengths (since BrC exhibits little or no absorption in this spectral region). Likewise, a unique combination of hematite and goethite exists that provides the “best” match to the AERONET retrieved refractive indices for the coarse mode.

Remote sensing of different absorbing aerosol species

G. L. Schuster et al.

Title Page

Abstract

Introduction

Conclusions

References

Tables

Figures



Back

Close

Full Screen / Esc

Printer-friendly Version

Interactive Discussion



Remote sensing of different absorbing aerosol species

G. L. Schuster et al.

Title Page

Abstract

Introduction

Conclusions

References

Tables

Figures



Back

Close

Full Screen / Esc

Printer-friendly Version

Interactive Discussion



Note that the host species is generally a mixture of components itself, with an unknown refractive index. Thus, we allow the real refractive index n_{host} to be a free parameter that is retrieved (unlike in Schuster et al., 2005, where we assumed that the host was water). We assume that all absorption is caused by sC, BrC, hematite, and goethite, and that therefore the host species is non-absorbing (i.e. $k_{\text{host}}(\lambda) = 0$). We also assume that the real refractive index of the host is spectrally flat ($dn_{\text{host}}/d\lambda = 0$). Finally, the real refractive index of BrC is not well characterized, so we assume that it has the same refractive index as the host aerosol (i.e., $n_{\text{BrC}} = n_{\text{host}}$).

2.1.1 Imaginary refractive index space for dust

We can use the Maxwell Garnett effective medium approximation (Bohren and Huffman, 1983) to determine the range of imaginary refractive indices expected for atmospheric dust that contains only hematite and goethite as absorbing species (i.e., no carbonaceous aerosols), which we present as the shaded area in Fig. 3. In this case, $f_1 = f_h$ is the volume fraction of hematite and $f_2 = f_g$ is the volume fraction of goethite. We use a real refractive index of 1.5 for the host aerosol, Chen and Cahan (1981) for the hematite refractive indices, Bedidi and Cervelle (1993) for the goethite refractive indices (see Table 1), and assume that all other minerals present have negligible absorption throughout the UV-NIR range of wavelengths. (We discuss the repercussions of using different refractive indices in the Sect. 4.) Field measurements indicate that free iron mass concentrations are less than about 5 % (Lafon et al., 2004; Wagner et al., 2012), so we present the range of computed refractive indices associated with up to 5 % free iron (by volume) as the shaded area in Fig. 3. The bottom border of the shaded area represents an $f_h = 0$ isoline and the top border represents an $f_g = 0$ isoline. Finally, the numbers along the top of the shaded area indicate the total percentage of free iron (i.e., hematite + goethite) on the vertical isolines (we also include an additional isoline outside of the shaded area for 10 % free iron).

2.1.2 Imaginary refractive index space for carbonaceous aerosols

In order to complete our description of two co-emitted aerosol absorbers in $k(440)$ vs. $k(670-1020)$ space, we similarly compute refractive indices for mixtures of carbonaceous aerosols. In this case, sC and BrC are the only absorbing species and $f_1 = f_{\text{sC}}$, $f_2 = f_{\text{BrC}}$. We use a spectrally invariant imaginary index of $m_{\text{sC}} = 1.95 + 0.79i$ for soot carbon (Bond and Bergstrom, 2006) and the Kirchstetter et al. (2004) measurements for BrC (see Fig. 1). The solid black line in Fig. 3 is a 1 : 1 line, and represents the spectrally invariant refractive index of soot carbon. The grey lines above the black line in Fig. 3 denote the contribution of brown carbon, with BrC/sC mass mixing ratios ranging from 1 to 20 (assuming that sC has a density of 1.8 g cm^{-3} and BrC has a density of 1.2 g cm^{-3} , as in Bond and Bergstrom, 2006; Turpin and Lim, 2001).

2.2 Separation of dust and carbonaceous aerosols

We are now in a position to evaluate the composition of the AERONET retrievals. We begin by assessing “pure” dust over the Middle East sites listed in Table 2, and plot AERONET Level 2 retrievals in Fig. 4a. We define “pure” dust as retrievals with fine mode volume fractions $\text{fvf} \leq 0.05$ and lidar depolarization ratios $\delta\rho \geq 0.2$ at the $0.532 \mu\text{m}$ wavelength (Schuster et al., 2012). Note that all of the retrievals in Fig. 4a lie in the shaded region, indicating that these AERONET retrievals are consistent with the free iron fractions found in the literature and the refractive indices that we used to compute the shaded region.

Similarly, we plot the AERONET retrievals from the South American sites during the peak of the biomass burning season in Fig. 4b. Note that these aerosols tend to have much higher imaginary indices at the red and near-infrared wavelengths (k_{rnr}) than the dust aerosols of Fig. 4a, and that most of the retrievals do not occupy the shaded area. This is because biomass burning aerosols are generally more absorbing than dust at $0.670-1.020 \mu\text{m}$. Also note that our retrieved BrC/sC mass ratio for biomass

Remote sensing of different absorbing aerosol species

G. L. Schuster et al.

[Title Page](#)[Abstract](#)[Introduction](#)[Conclusions](#)[References](#)[Tables](#)[Figures](#)[Back](#)[Close](#)[Full Screen / Esc](#)[Printer-friendly Version](#)[Interactive Discussion](#)

iron oxide by volume is roughly equivalent to 6.8 % iron oxide by mass, since the density of iron oxide is roughly twice that of other minerals (Formenti et al., 2014). Thus, this is consistent with the maximum 6.5 % free iron content measured by Lafon et al. (2006).

2.3 Aerosol layers with up to four absorbing species

5 We outlined the imaginary refractive index space occupied by dust and carbonaceous aerosols in Sect. 2.1. The absorption for both of these aerosol types can be described with two absorbing aerosol species (hematite and goethite for dust, organic and black carbon for carbonaceous aerosols). However, mixtures of dust with biomass burning require us to include four absorbers in the retrieval, which we discuss in this section.

10 Our basic approach is outlined in Fig. 6. Since carbonaceous aerosols are mainly found in the fine mode (radii $\lesssim 0.6 \mu\text{m}$), we initially assume that all sC and BrC are located in that mode. Likewise, iron oxides are mainly internally mixed with other minerals, and are the dominant absorbers in coarse mode dust (Sokolik and Toon, 1999; Lafon et al., 2006; Kandler et al., 2009; Wagner et al., 2012), so we initially assume that all hematite and goethite are located in the coarse mode. Unfortunately, we can not maintain all carbon in the fine mode and all iron oxide in the coarse mode for all aerosol retrievals; this is because AERONET provides a single refractive index for particles in both the fine and coarse modes, and sometimes the retrieved refractive indices can not be achieved with reasonable concentrations of a two-absorber mixture.

15 20 This conundrum is illustrated in Fig. 7, where we present all level 2.0 AERONET retrievals at the west Africa sites in k_{440} vs. k_{rnr} space. Aerosols at these sites include substantial concentrations of dust throughout the year, as well as seasonal biomass burning (Derimian et al., 2008). The points above the uppermost grey line in Fig. 7 would require BrC/sC mass ratios higher than 20 for the fine mode with our scheme (if we did not make an adjustment). However, the BrC/sC ratio is never greater than 15.2 for the South America biomass burning aerosols in Fig. 4b (this is also true for the South African biomass burning sites of Table 2). The retrievals with BrC/sC > 20

Remote sensing of different absorbing aerosol species

G. L. Schuster et al.

Title Page

Abstract

Introduction

Conclusions

References

Tables

Figures



Back

Close

Full Screen / Esc

Printer-friendly Version

Interactive Discussion



Remote sensing of different absorbing aerosol species

G. L. Schuster et al.

Title Page

Abstract

Introduction

Conclusions

References

Tables

Figures



Back

Close

Full Screen / Esc

Printer-friendly Version

Interactive Discussion



5 mixing ratios for these sites in the lower panels of Fig. 9. We show volume fractions this time (instead of column concentrations) to illustrate the intrinsic properties of the retrieval. Note that even though both African regions exhibit similar mixing ratios of iron oxides throughout the year (as shown in the lower panels of Fig. 9), the West African region has much higher iron oxide concentrations than the southern African region (as shown in the upper panels of Fig. 9). This is because the West African sites have a much stronger coarse mode than the southern African sites.

10 The lower left panel of Fig. 9 indicates that the volume fraction of free iron remains relatively constant in West Africa throughout the year (1.4–1.7 %). The carbonaceous signals, on the other hand, show a very strong seasonal variability, with sC and BrC peaking at 1.0 and 5.8 % for the fine mode during the winter biomass burning season. We see a similar pattern in southern Africa. That is, the coarse mode iron oxide mixing ratios are still steady throughout the year (at 1.1–1.3 %), and there's an obvious seasonal signal in the carbonaceous components of both modes, peaking at 3.0 % for sC and 3.7 % for BrC. The peak climatological volume mixing ratios for all four regions of Table 2 are listed in Table 3.

20 One can discern that BrC/sC volume ratio is always less than 2 at the South African sites of Fig. 9, and is sometimes less than 1; indeed, the median BrC/sC mass ratio is 0.7 during the peak of the biomass burning season. This is much lower than the organic/soot carbon mass ratios measured using in situ techniques, which typically range from 3 to 12 (Chen and Bond, 2010). However, in situ measurements are typically reported for measurements obtained close to sources and during fire events, but monthly averages represent periods between burns as well as the burn events; this could lower the BrC/sC ratios.

25 Additionally, in situ measurements typically account for all organic carbon (OC), whereas our retrieval is responsive only to organic species that have significant absorption at 0.440 μm . That is, BrC is part of OC (Moosmüller et al., 2009), so BrC concentrations are always less than OC concentrations, and BrC/sC < OC/sC. Alternatively, a greater proportion of OC could be encompassed by using a lower imaginary

Remote sensing of different absorbing aerosol species

G. L. Schuster et al.

Title Page

Abstract

Introduction

Conclusions

References

Tables

Figures



Back

Close

Full Screen / Esc

Printer-friendly Version

Interactive Discussion



refractive index for BrC; for instance, the median retrieved BrC/sC volume ratio increases from 1.5 to 2.7 for the South American biomass burning season when Chen and Bond (2010) is used for the BrC refractive index instead of Kirchstetter et al. (2004). However, the maximum BrC/sC value also increases from 15.2 to 27.5, and the latter value is well outside of the range outlined by Chen and Bond (2010).

Recently, some authors have attempted to use AAE to speciate carbonaceous aerosols and dust (Chung et al., 2012; Bahadur et al., 2012), so we present AAE vs. fine volume fraction (fvf) for the West Africa and South America sites in Fig. 10. The color code in each of the panels represents the volume fraction of one of the absorbing aerosol species with respect to the total volume of all absorbing aerosol species. The fraction of sC is presented in the top panel, BrC in the middle panel, and free iron in the lower panel. Data on the left side of the panels correspond to low fvf, and therefore are dominated by dust at the West African sites. Data on the right is dominated by biomass burning at the South American sites.

It is immediately obvious that the AAE parameter is sensitive to the relative proportions of sC and BrC when carbonaceous aerosols dominate the retrievals, as shown by the strong color gradients on the right side of the upper two panels. This is because of the strong spectral dependence of k_{BrC} and the wavelength-independent refractive index of sC shown in Fig. 1. The strong spectral dependence of k_{BrC} enhances the absorption at the shortest wavelengths, which increases AAE. Soot carbon has a wavelength-independent refractive index (Bond and Bergstrom, 2006; Bond et al., 2013), so the AAE of pure sC is smaller than the AAE of pure BrC for particles of the same size. Thus, both the AAE and our retrieved BrC are sensitive to the spectral dependence of the retrieved imaginary index, and the color gradient for carbonaceous aerosols in Fig. 10 reflects this.

However, Fig. 10 also indicates that AAE is not useful for discriminating between dust and carbonaceous aerosols. For instance, a retrieved AAE ~ 1.2 can not discriminate between the dust aerosols with fvf < 0.1 on the left side of Fig. 10 and the carbonaceous aerosols with fvf > 0.7 on the right side of Fig. 10. This is because the AAE of

pure dust has a large range of possible values (from less than 0 to greater than 3), depending upon the relative fractions of hematite and goethite. Thus, the AAE of dust is not well separated from the AAE of carbonaceous aerosols along the vertical axis in Fig. 10. This is discussed further in Schuster et al. (2015).

4 Sensitivity to component refractive indices

The refractive indices that we use for this retrieval are outlined in the upper portion of Table 1; refractive index uncertainty in any one of these components has an effect on all of the absorbing components to some extent, which we assess in this section. We assess this uncertainty by repeatedly retrieving sC, BrC, and hematite climatologies using all of the refractive index sources listed in Table 1, and then compare the results to our baseline retrieval. In order to stress the algorithm, we seek locations with significant concentrations of both dust and carbonaceous aerosols; thus, we use the month of January at the West African sites of Table 2. Dust is always present at those sites, and January is near the peak of the biomass burning season at those locations. We explain our baseline refractive index choices in Sect. 4.1; the sensitivity studies for sC, BrC, and free iron are presented in Sects. 4.2 and 4.3.

4.1 Rationale for our choice of baseline refractive indices

Bond and Bergstrom (2006) did an extensive review of sC refractive indices, and concluded that the available data was consistent with a constant refractive index at visible wavelengths. They also hypothesized that “strongly absorbing carbon with a single refractive index exists, and that some of the variation in reported refractive indices results from void fractions in the material.” They recommended using $k = 0.63\text{--}0.79$ for sC at visible wavelengths, favoring the larger extreme for highly graphitized carbon. The spectrally invariant value of $k_{sC} = 0.79$ was later adopted in Bond et al. (2013).

Remote sensing of different absorbing aerosol species

G. L. Schuster et al.

Title Page

Abstract

Introduction

Conclusions

References

Tables

Figures



Back

Close

Full Screen / Esc

Printer-friendly Version

Interactive Discussion



Thus, we use $m_{sC} = 1.95 + 0.79i$ at all wavelengths as our baseline complex refractive index for sC.

Reported values for the imaginary index of BrC varies by more than an order of magnitude at $\lambda = 0.440 \mu\text{m}$, as shown in Fig. 1 and Table 1. This is because BrC is a generic term for many absorbing organic carbon particles, and does not represent a single aerosol species, per se. The refractive index of BrC depends upon combustion conditions and the fuel source, and therefore can vary substantially between the various AERONET sites. We require that our BrC retrieval produces reasonable BrC fractions and BrC/sC ratios for all cases. So for instance, Table 4 indicates that using the lower limit of Sun et al. (2007) can result in f_{BrC} as high as 1.0 (i.e., 100 % brown carbon), which is clearly not acceptable. Fortunately, the refractive index of all BrC is negligible at the 670–1020 nm wavelengths (see Fig. 1), so BrC refractive index does not have a substantial impact on the retrieved sC mixing ratio (as shown in Sect. 4.2). We use Kirchstetter et al. (2004) for our baseline refractive index of BrC because it provides reasonable maximum and median f_{BrC} and BrC/sC ratios at the biomass burning sites.

Hematite also exhibits a large range of reported refractive indices, some of which are noted in Table 1. Hematite and goethite are the two dominant absorbers in mineral dust, and most of the spectral variability of dust absorption at visible wavelengths is associated with hematite. Consequently, we must choose a hematite source for our retrieval that has enough spectral variability to describe all of the AERONET retrievals. That is, k_{440}/k_{rmir} is often greater than 5 in the AERONET database, so we need to choose hematite and goethite optical properties that can accomplish this spectral variability. Since the only available goethite measurement has a positive spectral dependence (i.e., $dk/d\lambda > 0$, per Bedidi and Cerville, 1993), the hematite source that we choose must also indicate $k_{440}/k_{\text{rmir}} > 5$.

Additionally, our choice of mineral refractive indices must produce retrieved hematite and goethite fractions that are consistent with other work. In situ measurements indicate that hematite and goethite constitute 2.8–6.5 % of mineral dust by mass (Alfaro

Remote sensing of different absorbing aerosol species

G. L. Schuster et al.

[Title Page](#)[Abstract](#)[Introduction](#)[Conclusions](#)[References](#)[Tables](#)[Figures](#)[Back](#)[Close](#)[Full Screen / Esc](#)[Printer-friendly Version](#)[Interactive Discussion](#)

et al., 2004; Lafon et al., 2004, 2006; Wagner et al., 2012; Formenti et al., 2014). This corresponds to approximately 1.4–3.25 % by volume, since the density of iron oxide is much greater than other common minerals (4.28 g cm^{-3} for goethite and 5.25 g cm^{-3} for hematite, as opposed to 2.65 g cm^{-3} for illite, kaolinite, quartz, and calcite; Formenti et al., 2014). Additionally, the hematite fraction of free iron ranges from 17 to 61 % (Ji et al., 2002, 2004; Shi et al., 2012; Formenti et al., 2014).

We implemented the retrieval at the West Africa sites of Table 2, considering only “pure” dust (i.e., fine volume fractions less than 0.05 and depolarizations greater than 0.2), and present maximum and median results in Table 5. Here, we see that all of our candidate refractive indices for hematite produce median free iron and hematite fractions that are consistent with the in situ measurements, but only the Chen and Cahan (1981) refractive indices produce a maximum iron oxide fraction that is less than 3.5 %. Thus, we choose Chen and Cahan (1981) for our baseline retrieval, but we note that we have not scoured the literature for the most suitable hematite refractive index. The sensitivity of the results to our choice of refractive indices is discussed in the following two sections.

4.2 Sensitivity of retrieved sC to other absorbers

The sC results are shown in Fig. 11, which presents the relative mean biases with respect to the baseline value (i.e., $\overline{sC}/\overline{sC}_{\text{base}}$). The baseline retrieval is designated by the diamond in Fig. 11; it utilizes BrC refractive indices from Kirchstetter et al. (2004), hematite refractive indices from Chen and Cahan (1981), and sC refractive indices from Bond and Bergstrom (2006). We have included an additional six refractive indices for sC, BrC and hematite (as listed in the lower portion of Table 1), and tested 18 combinations of these component refractive indices. All of the retrievals utilize Bedidi and Cervelle (1993) for the refractive index of goethite, since that is the only source available for this mineral.

There are six groups of bars in Fig. 11. Each group of bars utilizes the same sC and BrC refractive indices, but different hematite refractive indices. Thus, the small

Remote sensing of different absorbing aerosol species

G. L. Schuster et al.

Title Page

Abstract

Introduction

Conclusions

References

Tables

Figures



Back

Close

Full Screen / Esc

Printer-friendly Version

Interactive Discussion



Remote sensing of different absorbing aerosol species

G. L. Schuster et al.

Title Page

Abstract

Introduction

Conclusions

References

Tables

Figures



Back

Close

Full Screen / Esc

Printer-friendly Version

Interactive Discussion



variability of the bars within each group indicates that the choice of hematite refractive index (as indicated by color) has very little effect on the sC retrieval ($\lesssim 1\%$). There are two reasons for this. (1) The retrieval initially assumes that sC and hematite are located in different modes (i.e., fine vs. coarse), so the absorption interference associated with these species is minimized; (2) the sC retrieval is mainly determined by the red and near-infrared wavelengths, and hematite has a much lower imaginary refractive index than sC at those wavelengths.

The two leftmost groups of bars in Fig. 11 utilize the same BrC refractive indices (i.e., Kirchstetter et al., 2004), so the dominant difference between these two groups is caused by the different sC refractive indices used for the retrievals. Groups of bars labeled “L” utilize $m_{\text{sC}} = 1.75 + 0.63i$, which is the low extreme from Bond and Bergstrom (2006); groups labeled “H” utilize $m_{\text{sC}} = 1.95 + 0.79i$, the highest recommended value of Bond and Bergstrom (2006). Thus, the full range of sC refractive indices recommended by Bond and Bergstrom (2006) produces a sC retrieval uncertainty of $\leq 14.2\%$.

We can assess the effect of k_{BrC} variability on the sC retrieval by observing all of the groups labeled “H” in Fig. 11. The retrievals in these four groups consistently use $k_{\text{sC}} = 0.79$, and the color code corresponds to the hematite refractive index. Consequently, the only differences between like-colored bars in the “H” groups is the BrC refractive index. Thus, the dark blue bars indicate that using Sun et al. (2007) water soluble organic carbon (WSOC) for the BrC refractive index produces the maximal relative bias of 5.8% below our baseline Kirchstetter et al. (2004) retrievals.

Some authors expected this value to be substantially higher (Ganguly et al., 2009), but BrC does not appreciably absorb radiation at red or near-infrared wavelengths (Jacobson, 1999; Sato et al., 2003; Kanakidou et al., 2005). Hence, it is actually quite easy to separate the effect of sC from BrC using refractive indices at the 670–1020 nm wavelengths, since sC absorption is more than 2 orders of magnitude greater than BrC absorption in this spectral region (as shown in Fig. 1).

Overall, Fig. 11 indicates that relative bias in the sC retrieval ranges from -5.8 to $+14.2\%$ at the African dust sites during the biomass burning season. The largest

and severs the link to the radiation field. Consequently, no known aerosol microphysical properties (i.e., component size distributions and complex refractive indices) can simultaneously describe the component AAOs that they report and the measured radiance fields in the AERONET database.

This last point is very important. AERONET provides a set of microphysical aerosol properties that can be used to accurately compute the radiance field at the surface. This link to the radiance field is the strength of the AERONET product, and therefore must be respected when we interpret the AERONET results. Reformulating the model assumptions in a manner that is not consistent with the original retrieval can produce results that are inconsistent with the radiance measurements. Thus, this lack of consistency with the AERONET retrieval model is an unaccounted source of error that still needs to be evaluated for the AAE and Bond techniques.

Our constrained refractive index approach is substantially different than the AAE and Bond approaches. Since we are constraining our retrievals to the AERONET refractive indices and using the same size distributions and forward modeling code to compute AAO as the operational AERONET algorithm, our column AAOs are constrained to the values reported by AERONET (and therefore have the same uncertainty). Because of this constraint, any uncertainty associated with sC refractive index or density does not propagate into sC AAO; rather, the retrieval adjusts the sC volume mixing ratio to maintain a mixture that matches the AERONET column refractive indices (and therefore AAO). Thus, the constrained refractive index approach results in identical sC AAOs for any assumed sC refractive index and density.

Consequently, the 15.4% uncertainty in sC volume fraction associated with uncertainty in the sC density and component refractive indices that we reported in Sect. 4.2 does NOT carry forward into the AAO computations. We can not emphasize this enough. That is, since our sC retrieval is constrained by the AERONET imaginary indices at the red and near-infrared wavelengths where it is the only absorbing aerosol species (e.g. Fig. 1, and Lindberg et al., 1993), the sC AAO associated with our retrievals is unaltered by the choice of sC density or refractive index. Additionally, our

Remote sensing of different absorbing aerosol species

G. L. Schuster et al.

Title Page

Abstract

Introduction

Conclusions

References

Tables

Figures



Back

Close

Full Screen / Esc

Printer-friendly Version

Interactive Discussion



approach provides a mass absorption cross section (MAC_{sC}) for each retrieval that can be checked against measurements and models. Finally, since our mixtures maintain the AERONET internal mixture assumption and are constrained by the AERONET refractive indices, our approach maintains a link to the measured radiance fields.

6 Conclusions

We present a method of distinguishing the relative concentrations soot carbon (sC), brown carbon, and iron oxide aerosol species in the atmosphere. The approach determines a mixture of absorbing and scattering aerosols that is consistent with the complex refractive indices provided by each AERONET retrieval. The method initially assumes that all carbonaceous aerosols are located in the fine aerosol mode, and that all iron oxides are located in the coarse aerosol mode. However, the retrieval allows some carbonaceous aerosols to populate the coarse mode, and some hematite to populate the fine mode (if this is necessary to reproduce the AERONET refractive indices). The solution for sC is unique because it is the only aerosol species with significant absorption at the red and near-infrared wavelengths. The solution for brown carbon and iron oxide is more ambiguous than the soot carbon retrieval, but the result for these other absorbers could be improved with better characterization of the refractive indices for those components.

The results show sensible regional and seasonal variability of the component aerosols, with the highest proportion of carbonaceous aerosols occurring at the seasonal biomass burning sites. The iron oxide mixing ratios and hematite/goethite ratios are also consistent with the values published in the scientific literature.

Our approach maintains the same internal mixture assumption that is employed by the operational AERONET product, and is constrained by the AERONET refractive indices; thus, there is a robust connection between our aerosol mixtures and the radiances measured with the AERONET sun photometers. This is not the case for the

Remote sensing of different absorbing aerosol species

G. L. Schuster et al.

Title Page

Abstract

Introduction

Conclusions

References

Tables

Figures



Back

Close

Full Screen / Esc

Printer-friendly Version

Interactive Discussion



Bond et al. (2013) and AAE approaches, which utilize external mixture assumptions for the absorbing aerosols.

We also present a sensitivity study, which indicates a 15.4 % uncertainty in retrieved sC concentration that is mainly associated with ambiguity of the sC refractive index documented in Bond and Bergstrom (2006). We note that this uncertainty in soot carbon mass does not carry forward to the sC AAOD or radiative forcing uncertainty, though. This is because the sC retrieval is constrained by the AERONET refractive indices at the red and near infrared wavelengths, where it is essentially the only absorbing aerosol. Consequently, the AAOD (and radiative forcing) computed using our sC retrieval and the AERONET size distribution matches the AERONET AAOD at those wavelengths, regardless of reasonable assumptions for the component aerosol refractive indices and densities.

Acknowledgements. This material was supported by the National Aeronautics and Space Administration under the NASA Glory Science Team, issued through the Science Mission Directorate, Earth Science Division. Oleg Dubovik was supported by the Labex CaPPA project involving several research institutions in Nord-Pas-de-Calais, France. Antti Arola acknowledges support from the Academy of Finland (through the project number 264242). We appreciate the efforts of the 29 AERONET and PHOTONS (Service d'Observation from LOA/USTL/CNRS) principal investigators and the entire AERONET and PHOTONS teams for obtaining, processing, documenting, and disseminating their respective datasets.

References

- Alfaro, S., Lafon, S., Rajot, J., Formenti, P., Gaudichet, A., and Maille, M.: Iron oxides and light absorption by pure desert dust: an experimental study, *J. Geophys. Res.*, 109, D08208, doi:10.1029/2003JD004374, 2004. 13624
- Andreae, M. O. and Gelencsér, A.: Black carbon or brown carbon? The nature of light-absorbing carbonaceous aerosols, *Atmos. Chem. Phys.*, 6, 3131–3148, doi:10.5194/acp-6-3131-2006, 2006. 13609

Remote sensing of different absorbing aerosol species

G. L. Schuster et al.

Title Page

Abstract

Introduction

Conclusions

References

Tables

Figures



Back

Close

Full Screen / Esc

Printer-friendly Version

Interactive Discussion



Remote sensing of different absorbing aerosol species

G. L. Schuster et al.

Title Page

Abstract

Introduction

Conclusions

References

Tables

Figures



Back

Close

Full Screen / Esc

Printer-friendly Version

Interactive Discussion



- Arimoto, R., Balsam, W., and Schloesslin, C.: Visible spectroscopy of aerosol particles collected on filters: iron-oxide minerals, *Atmos. Environ.*, 36, 89–96, 2002. 13612
- Arola, A., Schuster, G., Myhre, G., Kazadzis, S., Dey, S., and Tripathi, S. N.: Inferring absorbing organic carbon content from AERONET data, *Atmos. Chem. Phys.*, 11, 215–225, doi:10.5194/acp-11-215-2011, 2011. 13611
- Bahadur, R., Praveen, P., Xu, Y., and Ramanathan, V.: Solar absorption by elemental and brown carbon determined from spectral observations, *P. Natl. Acad. Sci. USA*, 109, 17366–17371, doi:10.1073/pnas.1205910109, 2012. 13611, 13622, 13628
- Bedidi, A. and Cervelle, B.: Light scattering by spherical particles with hematite and goethitelike optical properties: effect of water impregnation, *J. Geophys. Res.*, 98, 11941–11952, 1993. 13610, 13615, 13617, 13624, 13625, 13639, 13644
- Bohren, C. and Huffman, D.: *Absorption and Scattering of Light by Small Particles*, Wiley, New York, NY, USA, 1983. 13614, 13615
- Bond, T. and Bergstrom, R.: Light absorption by carbonaceous particles: an investigative review, *Aerosol Sci. Tech.*, 40, 27–67, 2006. 13609, 13616, 13622, 13623, 13625, 13626, 13627, 13631, 13639, 13644, 13654
- Bond, T., Doherty, S., Fahey, D., Forster, P., Berntsen, T., DeAngelo, B., Flanner, M., Ghan, S., Kärcher, B., Koch, D., Kinne, S., Kondo, Y., Quinn, P., Sarofim, M., Schultz, M., Schulz, M., Venkataraman, C., Zhang, H., Zhang, S., Bellouin, N., Guttikunda, S., Hopke, P., Jacobson, M., Kaiser, J., Klimont, Z., Lohmann, U., Schwarz, J., Shindell, D., Storelvmo, T., Warren, S., and Zender, C.: Bounding the role of black carbon in the climate system: a scientific assessment, *J. Geophys. Res.*, 118, 1–173, doi:10.1002/jgrd.50171, 2013. 13609, 13610, 13611, 13622, 13623, 13628, 13631
- Boucher, O., Randall, D., Artaxo, P., Bretherton, C., Feingold, G., Forster, P., Kerminen, V.-M., Kondo, Y., Liao, H., Lohmann, U., Rasch, P., Satheesh, S., Sherwood, S., Stevens, B., and Zhang, X.: Clouds and aerosols, in: *Climate Change 2013: the Physical Science Basis. Contribution of Working Group I to the Fifth Assessment Report of the Intergovernmental Panel on Climate Change*, edited by: Stocker, T. F., Qin, D., Plattner, G.-K., Tignor, M., Allen, S. K., Boschung, J., Nauels, A., Xia, Y., Bex, V., and Midgley, P. M., Cambridge University Press, Cambridge, UK, New York, NY, USA, 571–657, 2013. 13609
- Chakrabarty, R. K., Moosmüller, H., Chen, L.-W. A., Lewis, K., Arnott, W. P., Mazzoleni, C., Dubey, M. K., Wold, C. E., Hao, W. M., and Kreidenweis, S. M.: Brown carbon in tar balls from

**Remote sensing of
different absorbing
aerosol species**

G. L. Schuster et al.

Title Page

Abstract

Introduction

Conclusions

References

Tables

Figures



Back

Close

Full Screen / Esc

Printer-friendly Version

Interactive Discussion



smoldering biomass combustion, *Atmos. Chem. Phys.*, 10, 6363–6370, doi:10.5194/acp-10-6363-2010, 2010. 13612

Chen, C. and Cahan, B.: Visible and ultraviolet optical properties of single-crystal and polycrystalline hematite measured by spectroscopic ellipsometry, *J. Opt. Soc. Am.*, 71, 932–934, 1981. 13610, 13615, 13617, 13625, 13639, 13643, 13644

Chen, Y. and Bond, T. C.: Light absorption by organic carbon from wood combustion, *Atmos. Chem. Phys.*, 10, 1773–1787, doi:10.5194/acp-10-1773-2010, 2010. 13609, 13610, 13612, 13621, 13622, 13639, 13642, 13644

Chung, C., Ramanathan, V., and Decremer, D.: Observationally constrained estimates of carbonaceous aerosol radiative forcing, *P. Natl. Acad. Sci. USA*, 109, 11624–11629, 2012. 13609, 13611, 13622, 13628

Derimian, Y., Karnieli, A., Kaufman, Y. J., Andreae, M. O., Andreae, T. W., Dubovik, O., Maenhaut, W., and Koren, I.: The role of iron and black carbon in aerosol light absorption, *Atmos. Chem. Phys.*, 8, 3623–3637, doi:10.5194/acp-8-3623-2008, 2008. 13610, 13618, 13619

Dinar, E., AboRiziq, A., Spindler, C., Erlick, C., Kiss, G., and Rudich, Y.: The complex refractive index of atmospheric and model humic-like substances (HULIS) retrieved by a cavity ring down aerosol spectrometer (CRD-AS), *Faraday Discuss.*, 137, 279–295, 2008. 13609, 13612

Dubovik, O. and King, M.: A flexible inversion algorithm for retrieval of aerosol optical properties from sun and sky radiance measurements, *J. Geophys. Res.*, 105, 20673–20696, 2000. 13611, 13628

Dubovik, O., Smirnov, A., Holben, B., King, M., Kaufman, Y., Eck, T., and Slutsker, I.: Accuracy assessments of aerosol optical properties retrieved from Aerosol Robotic Network (AERONET) sun and sky radiance measurements, *J. Geophys. Res.*, 105, 9791–9806, 2000. 13611

Dubovik, O., Holben, B., Eck, T., Smirnov, A., Kaufman, Y., King, M., Tanre, D., and Slutsker, I.: Variability of absorption and optical properties of key aerosol types observed in worldwide locations, *J. Atmos. Sci.*, 59, 590–608, 2002. 13612

Formenti, P., Caquineau, S., Chevaillier, S., Klaver, A., Desboeufs, K., Rajot, J. L., Belin, S., and Briois, V.: Dominance of goethite over hematite in iron oxides of mineral dust from Western Africa: quantitative partitioning by X-ray absorption spectroscopy, *J. Geophys. Res.*, 119, 12740–12754, doi:10.1002/2014JD021668, 2014. 13612, 13618, 13625

Remote sensing of different absorbing aerosol species

G. L. Schuster et al.

Title Page

Abstract

Introduction

Conclusions

References

Tables

Figures



Back

Close

Full Screen / Esc

Printer-friendly Version

Interactive Discussion



- Ganguly, D., Ginoux, P., Ramaswamy, V., Dubovik, O., Welton, J., Reid, E., and Holben, B.: Inferring the composition and concentration of aerosols by combining AERONET and MPLNET data: comparison with other measurements and utilization to evaluate GCM output, *J. Geophys. Res.*, 114, D16203, doi:10.1029/2009JD011895, 2009. 13626
- 5 Gillespie, J. and Lindberg, J.: Ultraviolet and visible imaginary refractive index of strongly absorbing atmospheric particulate matter, *Appl. Optics*, 31, 2112–2115, 1992. 13610, 13639, 13643, 13644
- Ginoux, P., Prospero, J., Gill, T., Hsu, N., and Zhao, M.: Global-scale attribution of anthropogenic and natural dust sources and their emission rates based on MODIS Deep Blue aerosol products, *Rev. Geophys.*, 50, RG3005, doi:10.1029/2012RG000388, 2012. 13617
- 10 Hand, V., Capes, G., Vaughan, D., Formenti, P., Haywood, J., and Coe, H.: Evidence of internal mixing of African dust and biomass burning particles by individual particle analysis using electron beam techniques, *J. Geophys. Res.*, 115, D13301, doi:10.1029/2009JD012938, 2010. 13619
- 15 Hoffer, A., Gelencsér, A., Guyon, P., Kiss, G., Schmid, O., Frank, G. P., Artaxo, P., and Andreae, M. O.: Optical properties of humic-like substances (HULIS) in biomass-burning aerosols, *Atmos. Chem. Phys.*, 6, 3563–3570, doi:10.5194/acp-6-3563-2006, 2006. 13609, 13612
- Holben, B., Eck, T., Slutsker, I., Tanre, D., Buis, J., Setzer, A., Vermote, E., Reagan, J., Kaufman, Y., Nakajima, T., Lavenue, F., Jankowiak, I., and Smirnov, A.: AERONET – a federated instrument network and data archive for aerosol characterization, *Remote Sens. Environ.*, 66, 1–16, 1998. 13611
- 20 Holben, B., Tanre, D., Smirnov, A., Eck, T., Slutsker, I., Abuhassan, N., Newcomb, W., Schafer, J., Chatenet, B., Lavenue, F., Kaufman, Y., Castle, J. V., Setzer, A., Markham, B., Clark, D., Frouin, R., Halthore, R., Karneli, A., O'Neill, N., Pietras, C., Pinker, R., Voss, K., and Zibordi, G.: An emerging ground-based aerosol climatology: aerosol optical depth from AERONET, *J. Geophys. Res.*, 106, 12067–12097, 2001. 13611
- 25 Hsu, W. and Matijević, E.: Optical properties of monodispersed hemitite hydrosols, *Appl. Optics*, 24, 1623–1630, 1985. 13610, 13627, 13639, 13643, 13644
- 30 Jacobson, M.: Isolating nitrated and aromatic aerosols and nitrated aromatic gases as sources of ultraviolet light absorption, *J. Geophys. Res.*, 106, 3527–3542, 1999. 13609, 13626

**Remote sensing of
different absorbing
aerosol species**

G. L. Schuster et al.

[Title Page](#)[Abstract](#)[Introduction](#)[Conclusions](#)[References](#)[Tables](#)[Figures](#)[Back](#)[Close](#)[Full Screen / Esc](#)[Printer-friendly Version](#)[Interactive Discussion](#)

Jacobson, M.: Short-term effects of controlling fossil-fuel soot, biofuel soot and gases, and methane on climate, Arctic ice, and air pollution health, *J. Geophys. Res.*, 115, D14209, doi:10.1029/2009JD013795, 2010. 13610

Ji, J., Balsam, W., Chen, J., and Liu, L.: Rapid and quantitative measurement of hematite and goethite in the Chinese loess-paleosol sequence by diffuse reflectance spectroscopy, *Clay Clay Miner.*, 50, 208–216, 2002. 13625

Ji, J., Chen, J., Balsam, W., Lu, H., Sun, Y., and Xu, H.: High resolution hematite/goethite records from Chinese loess sequences for the last glacial–interglacial cycle: rapid climatic response of the East Asian Monsoon to the tropical Pacific, *Geophys. Res. Lett.*, 31, L03207, doi:10.1029/2003GL018975, 2004. 13625

Kanakidou, M., Seinfeld, J. H., Pandis, S. N., Barnes, I., Dentener, F. J., Facchini, M. C., Van Dingenen, R., Ervens, B., Nenes, A., Nielsen, C. J., Swietlicki, E., Putaud, J. P., Balkanski, Y., Fuzzi, S., Horth, J., Moortgat, G. K., Winterhalter, R., Myhre, C. E. L., Tsigaridis, K., Vignati, E., Stephanou, E. G., and Wilson, J.: Organic aerosol and global climate modelling: a review, *Atmos. Chem. Phys.*, 5, 1053–1123, doi:10.5194/acp-5-1053-2005, 2005. 13609, 13626

Kandler, K., Benker, N., Bundke, U., Cuevas, E., Ebert, M., Knippertz, P., Rodriguez, S., Schütz, L., and Weinbruch, S.: Chemical composition and complex refractive index of Saharan mineral dust at Izaña, Tenerife (Spain) derived by electron microscopy, *Atmos. Environ.*, 41, 8058–8074, 2007. 13619

Kandler, K., Schütz, L., Deutscher, C., Ebert, M., Hofmann, H., Jäckel, S., Jaenicke, R., Knippertz, P., Lieke, K., Massling, A., Petzold, A., Schladitz, A., Weinzierl, B., Wiedensohler, A., Zorn, S., and Weinbruch, S.: Size distribution, mass concentration, chemical and mineralogical composition and derived optical parameters of the boundary layer aerosol at Tinfou, Morocco, during SAMUM 2006, *Tellus B*, 61, 32–50, 2009. 13618

Kerker, M., Scheiner, P., Cooke, D., and Kratochvil, J.: Absorption index and color of colloidal hematite, *J. Colloid Interf. Sci.*, 71, 176–187, 1979. 13610, 13627, 13639

Kim, D., Chin, M., Yu, H., Eck, T. F., Sinyuk, A., Smirnov, A., and Holben, B. N.: Dust optical properties over North Africa and Arabian Peninsula derived from the AERONET dataset, *Atmos. Chem. Phys.*, 11, 10733–10741, doi:10.5194/acp-11-10733-2011, 2011. 13612

Kirchstetter, T., Novakov, T., and Hobbs, P.: Evidence that spectral dependence of light absorption by aerosols is affected by organic carbon, *J. Geophys. Res.*, 109, D21208,

Remote sensing of different absorbing aerosol species

G. L. Schuster et al.

Title Page

Abstract

Introduction

Conclusions

References

Tables

Figures



Back

Close

Full Screen / Esc

Printer-friendly Version

Interactive Discussion



doi:10.1029/2004JD004999, 2004. 13609, 13610, 13612, 13616, 13622, 13624, 13625, 13626, 13639, 13642, 13644

Koch, D., Schulz, M., Kinne, S., McNaughton, C., Spackman, J. R., Balkanski, Y., Bauer, S., Berntsen, T., Bond, T. C., Boucher, O., Chin, M., Clarke, A., De Luca, N., Dentener, F., Diehl, T., Dubovik, O., Easter, R., Fahey, D. W., Feichter, J., Fillmore, D., Freitag, S., Ghan, S., Ginoux, P., Gong, S., Horowitz, L., Iversen, T., Kirkevåg, A., Klimont, Z., Kondo, Y., Krol, M., Liu, X., Miller, R., Montanaro, V., Moteki, N., Myhre, G., Penner, J. E., Perlwitz, J., Pitari, G., Reddy, S., Sahu, L., Sakamoto, H., Schuster, G., Schwarz, J. P., Seland, Ø., Stier, P., Takegawa, N., Takemura, T., Textor, C., van Aardenne, J. A., and Zhao, Y.: Evaluation of black carbon estimations in global aerosol models, *Atmos. Chem. Phys.*, 9, 9001–9026, doi:10.5194/acp-9-9001-2009, 2009. 13610

Koven, C. and Fung, I.: Inferring dust composition from wavelength-dependent absorption in Aerosol Robotic Network AERONET data, *J. Geophys. Res.*, 111, D14205, doi:10.1029/2005JD006678, 2006. 13611

Lack, D., Richardson, M., Law, D., Langridge, J., Cappa, C., McLaughlin, R., and Murphy, D.: Aircraft instrument for comprehensive characterization of aerosol optical properties, Part 2: Black and brown carbon absorption and absorption enhancement measured with photo acoustic spectroscopy, *Aerosol Sci. Tech.*, 46, 555–568, 2012. 13612

Lafon, S., Rajot, J.-L., Alfaro, S., and Gaudichet, A.: Quantification of iron oxides in desert aerosol, *Atmos. Environ.*, 38, 1211–1218, 2004. 13615, 13625

Lafon, S., Sokolik, I., Rajot, J., Caquineau, S., and Gaudichet, A.: Characterization of iron oxides in mineral dust aerosols: implications for light absorption, *J. Geophys. Res.*, 111, D21207, doi:10.1029/2005JD007016, 2006. 13612, 13618, 13625

Lesins, G., Chylek, P., and Lohmann, U.: A study of internal and external mixing scenarios and its effect on aerosol optical properties and direct radiative forcing, *J. Geophys. Res.*, 107, 4094, doi:10.1029/2001JD000973, 2002. 13614

Li, Z., Gu, X., Wang, L., Li, D., Xie, Y., Li, K., Dubovik, O., Schuster, G., Goloub, P., Zhang, Y., Li, L., Ma, Y., and Xu, H.: Aerosol physical and chemical properties retrieved from ground-based remote sensing measurements during heavy haze days in Beijing winter, *Atmos. Chem. Phys.*, 13, 10171–10183, doi:10.5194/acp-13-10171-2013, 2013. 13611

Lindberg, J. D., Douglass, R. E., and Garvey, D. M.: Carbon and the optical properties of atmospheric dust, *Appl. Optics*, 32, 6077–6081, 1993. 13629

Remote sensing of different absorbing aerosol species

G. L. Schuster et al.

Title Page

Abstract

Introduction

Conclusions

References

Tables

Figures



Back

Close

Full Screen / Esc

Printer-friendly Version

Interactive Discussion



Malm, W., Sisler, J., Huffman, D., Eldred, R., and Cahill, T.: Spatial and seasonal trends in particle concentration and optical extinction in the United States, *J. Geophys. Res.*, 99, 1347–1370, 1994. 13610

Moosmüller, H., Chakrabarty, R., and Arnott, W.: Aerosol light absorption and its measurement: a review, *J. Quant. Spectrosc. Ra*, 110, 844–878, 2009. 13621

Myhre, G., Samset, B. H., Schulz, M., Balkanski, Y., Bauer, S., Bernsten, T. K., Bian, H., Bellouin, N., Chin, M., Diehl, T., Easter, R. C., Feichter, J., Ghan, S. J., Hauglustaine, D., Iversen, T., Kinne, S., Kirkevåg, A., Lamarque, J.-F., Lin, G., Liu, X., Lund, M. T., Luo, G., Ma, X., van Noije, T., Penner, J. E., Rasch, P. J., Ruiz, A., Seland, Ø., Skeie, R. B., Stier, P., Takemura, T., Tsigaridis, K., Wang, P., Wang, Z., Xu, L., Yu, H., Yu, F., Yoon, J.-H., Zhang, K., Zhang, H., and Zhou, C.: Radiative forcing of the direct aerosol effect from AeroCom Phase II simulations, *Atmos. Chem. Phys.*, 13, 1853–1877, doi:10.5194/acp-13-1853-2013, 2013a. 13609

Myhre, G., Shindell, D., Brèon, F.-M., Collins, W., Fuglestedt, J., Huang, J., Koch, D., Lamarque, J.-F., Lee, D., Mendoza, B., Nakajima, T., Robock, A., Stephens, G., Takemura, T., and Zhang, H.: Anthropogenic and natural radiative forcing, in: *Climate Change 2013: The Physical Science Basis. Contribution of Working Group I to the Fifth Assessment Report of the Intergovernmental Panel on Climate Change*, edited by: Stocker, T. F., Qin, D., Plattner, G.-K., Tignor, M., Allen, S. K., Boschung, J., Nauels, A., Xia, Y., Bex, V., and Midgley, P. M., Cambridge University Press, Cambridge, UK, New York, NY, USA, 659–740, 2013b. 13609

Park, R., Jacob, D., Chin, M., and Martin, R.: Sources of carbonaceous aerosols over the United States and implications for natural visibility, *J. Geophys. Res.*, 108, 4355, doi:10.1029/2002JD003190, 2003. 13610

Ramanathan, V. and Carmichael, G.: Global and regional climate changes due to black carbon, *Nat. Geosci.*, 1, 221–227, doi:10.1038/ngeo156, 2008. 13609

Sato, M., Hansen, J., Koch, D., Lacis, A., Ruedy, R., Dubovik, O., Holben, B., Chin, M., and Novakov, T.: Global atmospheric black carbon inferred from AERONET, *P. Natl. Acad. Sci. USA*, 100, 6319–6324, 2003. 13610, 13626

Schnaiter, M., Gimmler, M., Llamas, I., Linke, C., Jäger, C., and Mutschke, H.: Strong spectral dependence of light absorption by organic carbon particles formed by propane combustion, *Atmos. Chem. Phys.*, 6, 2981–2990, doi:10.5194/acp-6-2981-2006, 2006. 13609

Schuster, G. L., Dubovik, O., Holben, B. N., and Clothiaux, E. E.: Inferring black carbon content and specific absorption from Aerosol Robotic Network (AERONET) aerosol retrievals, *J.*

**Remote sensing of
different absorbing
aerosol species**

G. L. Schuster et al.

[Title Page](#)[Abstract](#)[Introduction](#)[Conclusions](#)[References](#)[Tables](#)[Figures](#)[Back](#)[Close](#)[Full Screen / Esc](#)[Printer-friendly Version](#)[Interactive Discussion](#)

Geophys. Res., 110, D10S17, doi:10.1029/2004JD004548, 2005. 13611, 13613, 13614, 13615, 13628

Schuster, G. L., Vaughan, M., MacDonnell, D., Su, W., Winker, D., Dubovik, O., Lapyonok, T., and Trepte, C.: Comparison of CALIPSO aerosol optical depth retrievals to AERONET measurements, and a climatology for the lidar ratio of dust, *Atmos. Chem. Phys.*, 12, 7431–7452, doi:10.5194/acp-12-7431-2012, 2012. 13616, 13617

Schuster, G. L., Dubovik, O., and Arola, A.: Remote sensing of soot carbon, Part 2: Understanding the absorption Angstrom exponent, *Atmos. Chem. Phys. Discuss.*, in review, 2015. 13611, 13619, 13623

Schwarz, J., Spackman, J., Gao, R., Watts, L., Stier, P., Schulz, M., Davis, S., Wofsy, S., and Fehy, D.: Global-scale black carbon profiles observed in the remote atmosphere and compared to models, *Geophys. Res. Lett.*, 37, L18812, doi:10.1029/2010GL044372, 2010. 13610

Shi, Z., Krom, M., Jickells, T., Bonneville, S., Carslaw, K., Mihalopoulos, N., Baker, A., and Benning, L.: Impacts on iron solubility in the mineral dust by processes in the source region and the atmosphere: a review, *Aeolian Res.*, 5, 21–42, 2012. 13612, 13625

Sokolik, I. and Toon, O.: Incorporation of mineralogical composition into models of the radiative properties of mineral aerosol from UV to IR wavelengths, *J. Geophys. Res.*, 104, 9423–9444, 1999. 13618

Sun, H., Biedermann, L., and Bond, T.: Color of brown carbon: a model for ultraviolet and visible light absorption by organic carbon aerosol, *Geophys. Res. Lett.*, 34, L17813, doi:10.1029/2007GL029797, 2007. 13609, 13610, 13612, 13624, 13626, 13627, 13639, 13642, 13644

Turpin, B. and Lim, H.-J.: Species contributions to $PM_{2.5}$ mass concentrations: revisiting common assumptions for estimating organic mass, *Aerosol Sci. Tech.*, 35, 602–610, 2001. 13616

Wagner, R., Ajtai, T., Kandler, K., Lieke, K., Linke, C., Müller, T., Schnaiter, M., and Vragel, M.: Complex refractive indices of Saharan dust samples at visible and near UV wavelengths: a laboratory study, *Atmos. Chem. Phys.*, 12, 2491–2512, doi:10.5194/acp-12-2491-2012, 2012. 13612, 13615, 13618, 13625

Wang, L., Li, Z., Tian, Q., Ma, Y., Zhang, F., Zhang, Y., Li, D., Li, K., and Li, L.: Estimate of aerosol absorbing components of black carbon, brown carbon, and dust from ground-based remote sensing data of sun-sky radiometers, *J. Geophys. Res.*, 118, 6534–6543, doi:10.1002/jgrd.50356, 2013. 13611

Remote sensing of
different absorbing
aerosol species

G. L. Schuster et al.

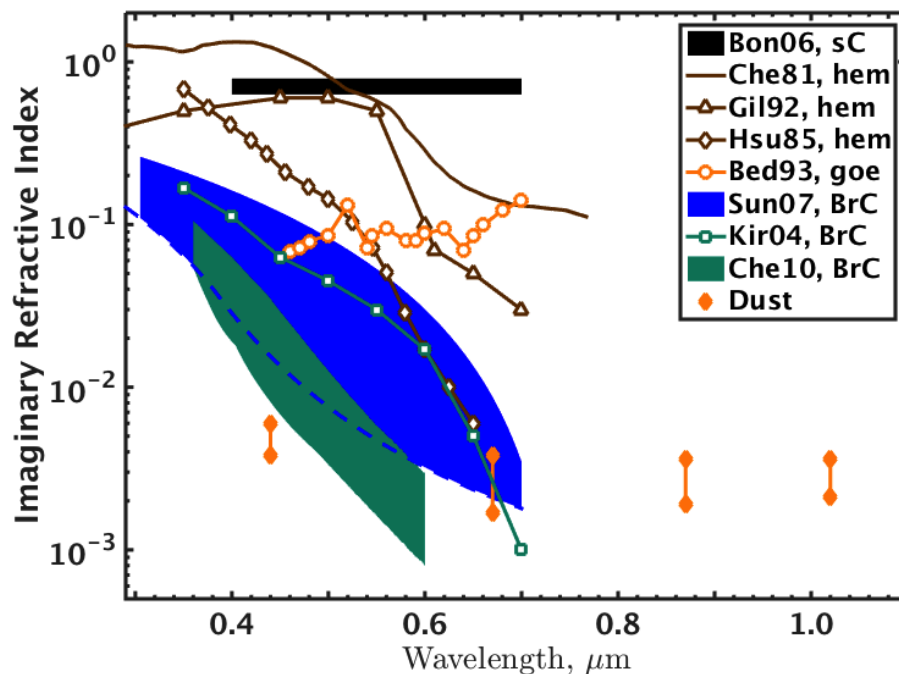


Figure 1. Imaginary refractive index of several absorbing aerosols. Bon06 – soot carbon (Bond and Bergstrom, 2006); Che81 – hematite (Chen and Cahan, 1981); Gil92 – hematite (Gillespie and Lindberg, 1992); Hsu85 – hematite (Hsu and Matijević, 1985); Bed93 – goethite (Bedidi and Cervelle, 1993); Sun07 – brown carbon (Sun et al., 2007); Kir04 – brown carbon (Kirchstetter et al., 2004); Che10 – brown carbon (Chen and Bond, 2010); Dust – range of AERONET dust climatologies over Africa and the Middle East.

Title Page

Abstract

Introduction

Conclusions

References

Tables

Figures



Back

Close

Full Screen / Esc

Printer-friendly Version

Interactive Discussion



Remote sensing of different absorbing aerosol species

G. L. Schuster et al.

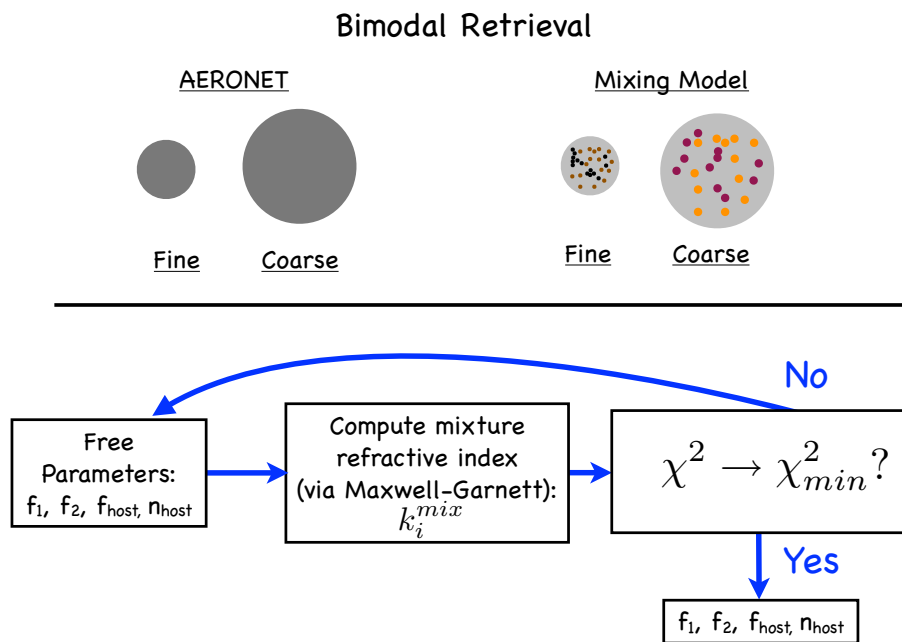


Figure 2. Schematic illustrating carbonaceous aerosol retrieval (sC and BrC) for the fine mode and free iron retrieval (goethite and hematite) for the coarse mode. AERONET provides refractive indices for uniform particles, and the retrieval uses different components for each mode to find a mixture that matches the AERONET refractive indices.

Title Page	
Abstract	Introduction
Conclusions	References
Tables	Figures
⏪	⏩
⏴	⏵
Back	Close
Full Screen / Esc	
Printer-friendly Version	
Interactive Discussion	



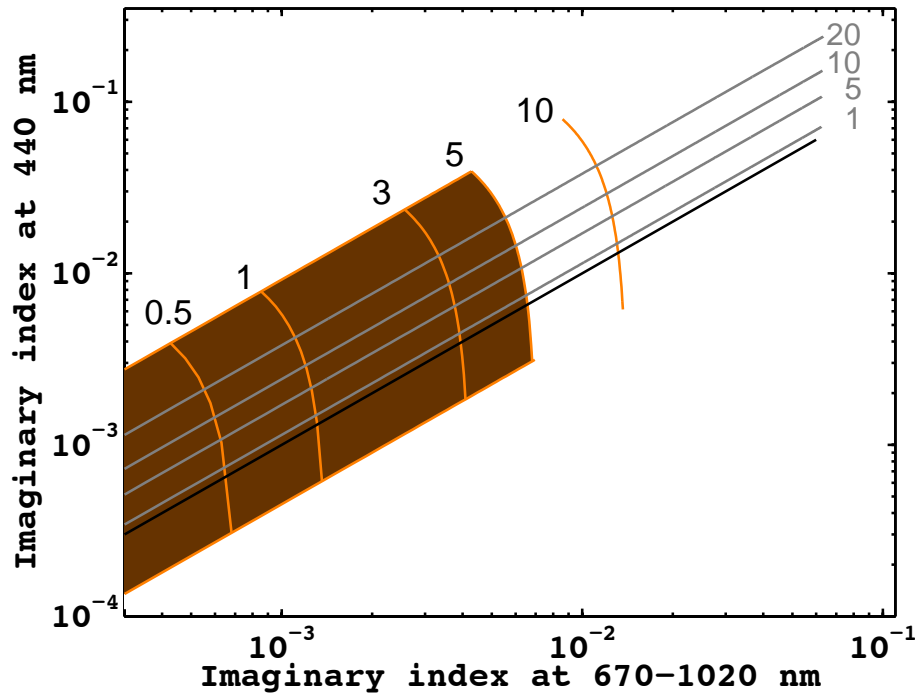


Figure 3. Shaded area indicates imaginary refractive indices at the AERONET wavelengths that are possible with mixtures of 0–5 % by volume of iron oxide in the form of hematite and/or goethite (as denoted by the orange isolines). The bottom border of the shaded area represents a 0% hematite isoline, and the top border represents a 0% goethite isoline. The x axis is an average for the 670, 870, and 1020 nm wavelengths. Solid black line presents spectrally invariant refractive index, as expected for black carbon. Solid grey lines indicate OC/BC mass mixing ratios of 1, 5, 10, and 20 when no absorbing dust is present.

Remote sensing of different absorbing aerosol species

G. L. Schuster et al.

Title Page	
Abstract	Introduction
Conclusions	References
Tables	Figures
◀	▶
◀	▶
Back	Close
Full Screen / Esc	
Printer-friendly Version	
Interactive Discussion	



Remote sensing of different absorbing aerosol species

G. L. Schuster et al.

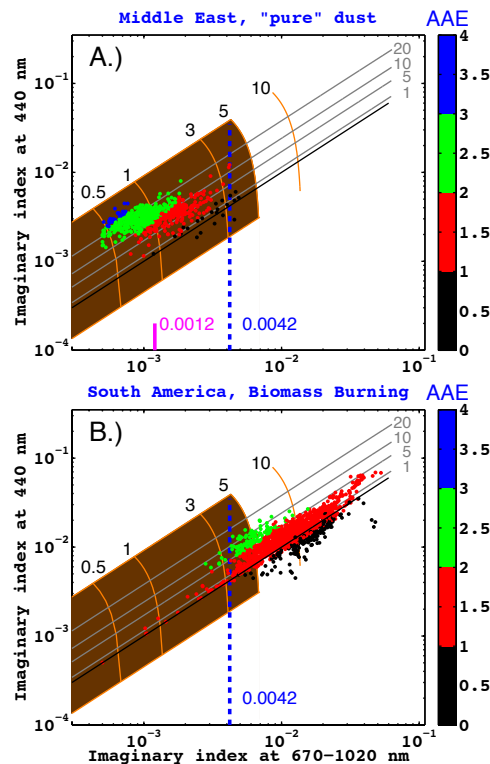


Figure 4. AERONET Level 2.0 imaginary refractive index at 440 nm vs. the 670–1020 nm average; color code corresponds to the absorption Angstrom exponent. Top panel: data over the Middle East, filtered to retain only dust (i.e., require fine volume fractions less than 0.05 and depolarizations greater than 0.2 at the 532 nm wavelength). Vertical magenta line denotes the median. Bottom panel: South America biomass burning sites for August and September. The vertical dashed line at $k(670\text{--}1020) = 0.0042$ separates 95 % of the two datasets. See Table 2 for a listing of AERONET sites used in these regions.

Title Page

Abstract

Introduction

Conclusions

References

Tables

Figures



Back

Close

Full Screen / Esc

Printer-friendly Version

Interactive Discussion



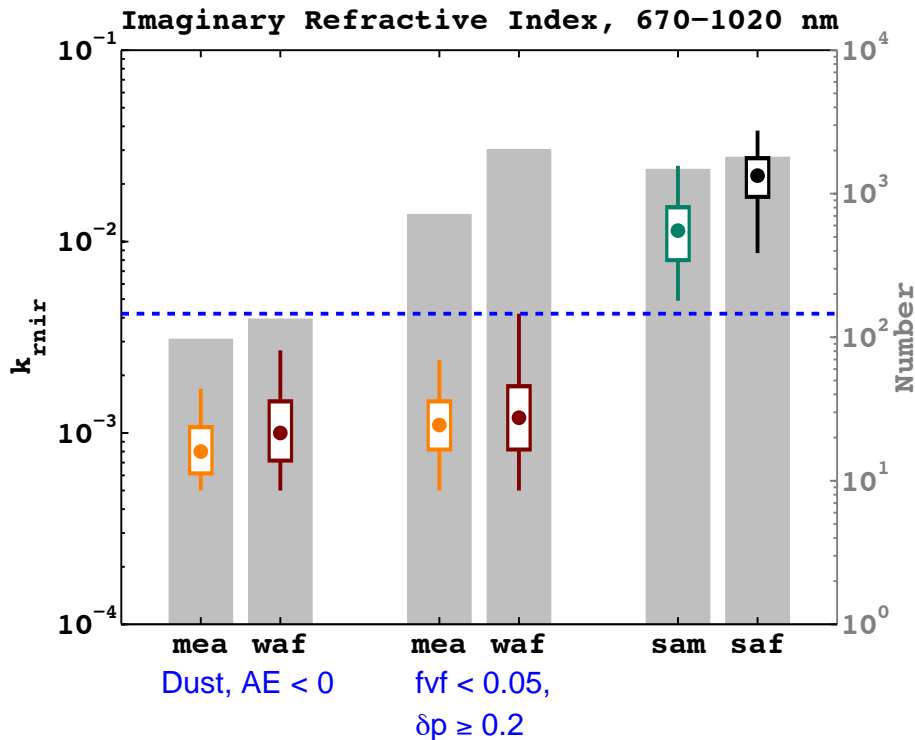


Figure 5. Boxplots for the Level 2.0 imaginary refractive indices averaged over the 670–1020 nm wavelengths at the AERONET sites listed in Table 2. Circles represent medians, box edges are the 25th and 75th percentiles, whisker ends are the 5th and 95th percentiles. Grey bars indicate the number of data points contributing to each boxplot. The Middle East (mea) and west Africa (waf) sites are filtered for dust using two different methods. Biomass burning sites are considered only during the peak of the biomass burning seasons (August–September for South America, or sam; July–September for South Africa, or saf). The dashed blue line illustrates that $k_{rnir} = 0.0042$ separates at least 95 % of the dust and biomass imaginary refractive indices.

Remote sensing of different absorbing aerosol species

G. L. Schuster et al.

Title Page	
Abstract	Introduction
Conclusions	References
Tables	Figures
◀	▶
◀	▶
Back	Close
Full Screen / Esc	
Printer-friendly Version	
Interactive Discussion	



Remote sensing of
different absorbing
aerosol species

G. L. Schuster et al.

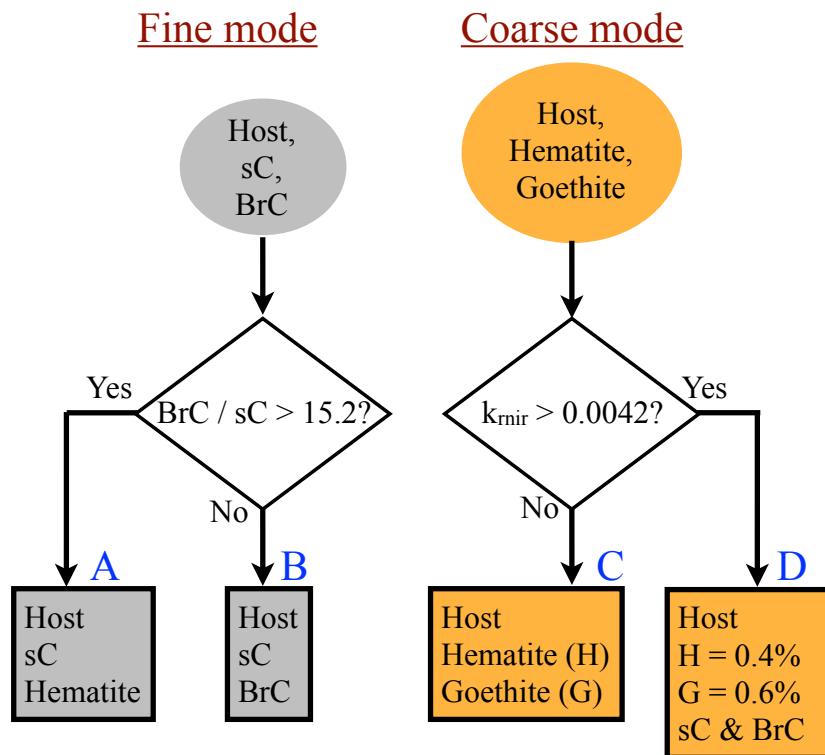


Figure 6. Flowchart showing absorbing aerosol retrieval process. Initially, all carbonaceous species are assumed to occupy the fine mode and all iron oxide (hematite, goethite) is assumed to occupy the coarse mode. If $\text{BrC}/\text{sC} > 15.2$ would be required for a 2-component mixture, then hematite is used instead of BrC to characterize the spectral dependence of the refractive index in the fine mode (branch A). Likewise, if the retrieved absorption at the red and near-infrared wavelengths is above a threshold of $k_{\text{rmir}} = 0.0042$, then the hematite and goethite fractions are fixed at the values we retrieved for “pure” African dust, and some carbonaceous aerosol is assumed to occupy the coarse mode (branch D).

Title Page	
Abstract	Introduction
Conclusions	References
Tables	Figures
◀	▶
◀	▶
Back	Close
Full Screen / Esc	
Printer-friendly Version	
Interactive Discussion	



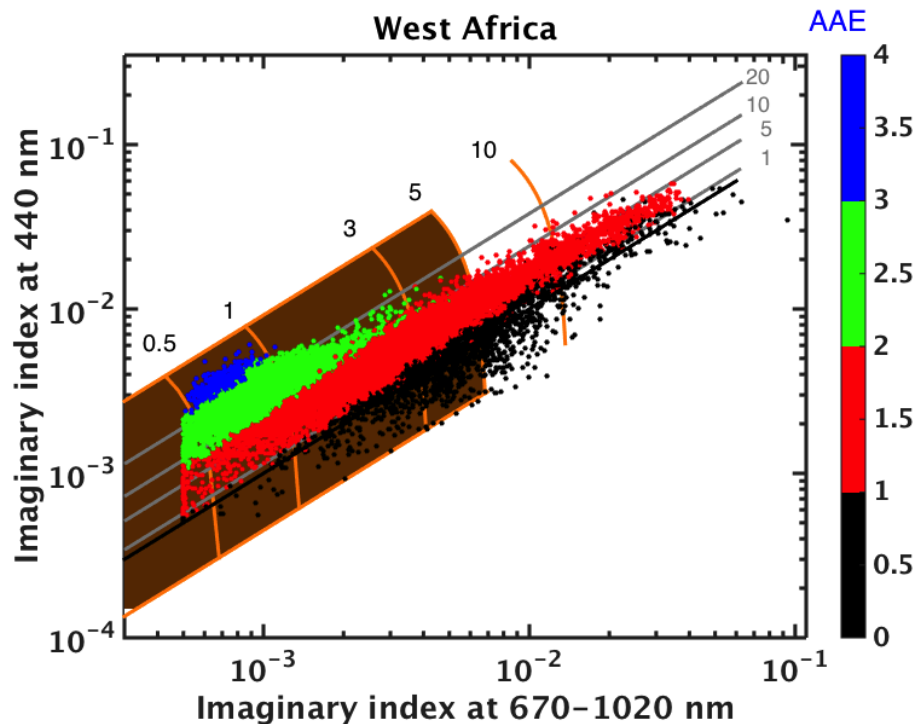


Figure 7. All level 2.0 retrievals for the West African AERONET sites of Table 2, including mixtures of biomass burning and dust. Many of the points are located above the uppermost grey line, which would require BrC/sC ratios greater than 15.2 for a mixture containing only carbonaceous aerosols. Likewise, retrievals to the right of the shaded area require iron oxide volume mixing ratios greater than 5% if no carbonaceous aerosol is included.

Remote sensing of different absorbing aerosol species

G. L. Schuster et al.

Title Page

Abstract Introduction

Conclusions References

Tables Figures

◀ ▶

◀ ▶

Back Close

Full Screen / Esc

Printer-friendly Version

Interactive Discussion



Remote sensing of
different absorbing
aerosol species

G. L. Schuster et al.

Title Page

Abstract

Introduction

Conclusions

References

Tables

Figures



Back

Close

Full Screen / Esc

Printer-friendly Version

Interactive Discussion

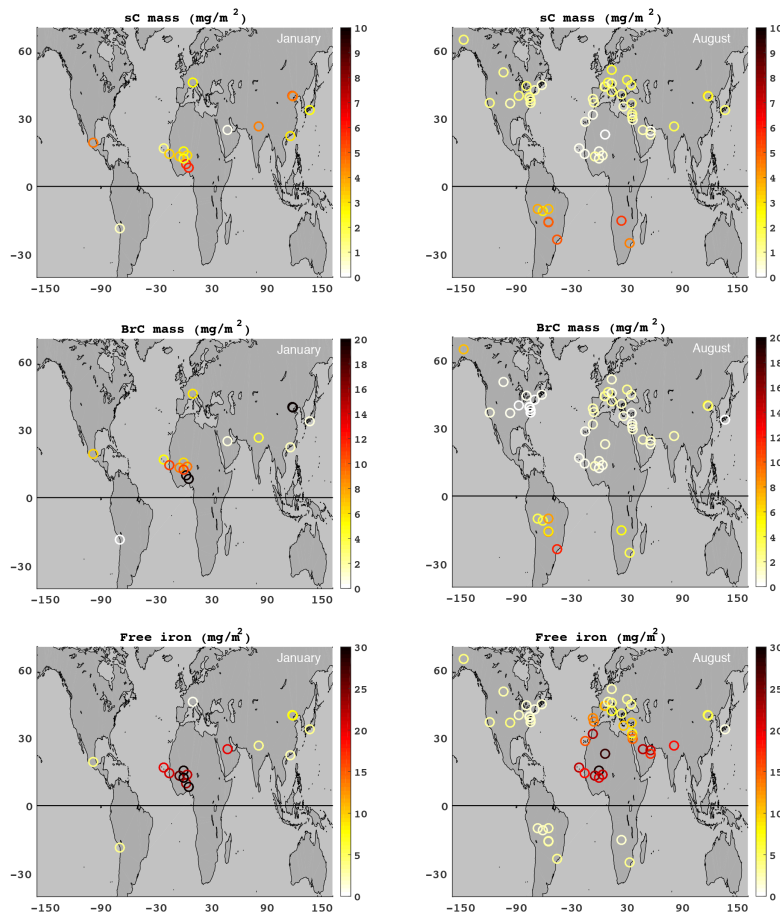


Figure 8. Column mass concentrations of sC (top row), BrC (middle row), and iron oxide (bottom row) retrieved from Level 2.0 AERONET data for January (left column) and August (right column). Minimum number of retrievals is 25 for each site.

Remote sensing of different absorbing aerosol species

G. L. Schuster et al.

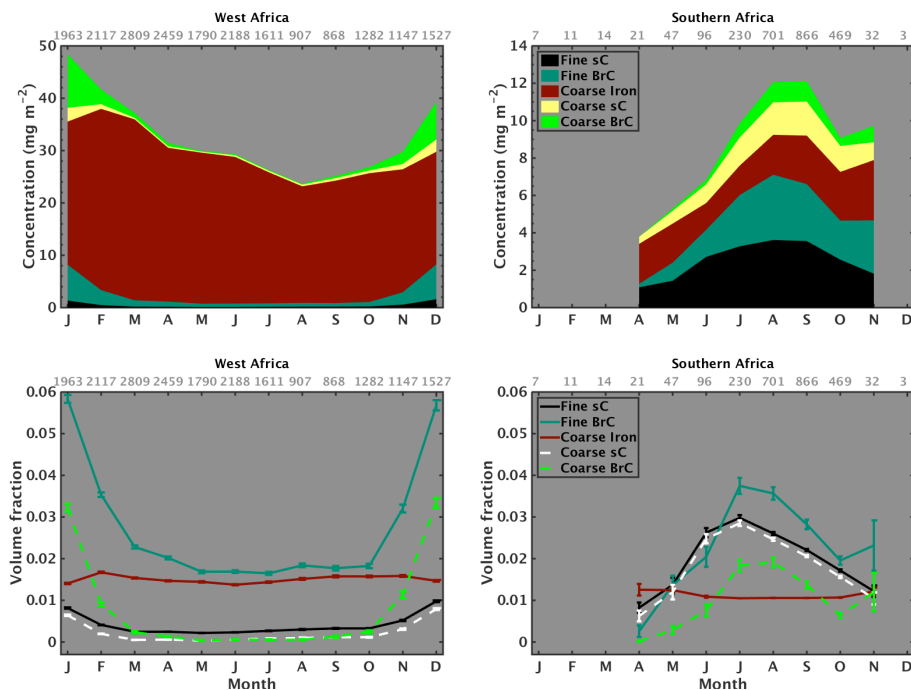


Figure 9. Upper panels: monthly-averaged column concentrations of retrieved sC, BrC, and free iron in the fine and coarse modes at the West Africa and southern African sites (fine mode iron is negligible at these scales). Note the difference in y axis scales. Lower panels: monthly averaged volume fractions at the same sites. Error bars represent the SD of the means. Number of retrievals per month shown along upper axes; only months with more than 20 retrievals are shown in plots.

Remote sensing of different absorbing aerosol species

G. L. Schuster et al.

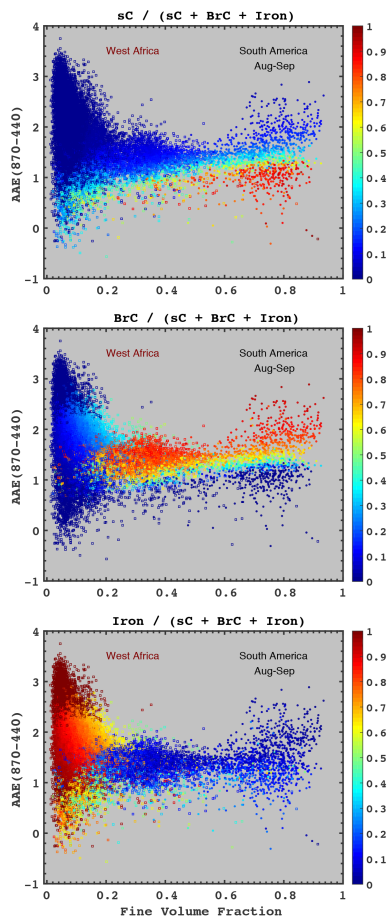


Figure 10. Colormaps showing the volume fraction of absorbing species associated with each absorber. Data located mainly on the left is from the West African sites, data on the right corresponds to the biomass burning season at the South American sites.

Remote sensing of different absorbing aerosol species

G. L. Schuster et al.

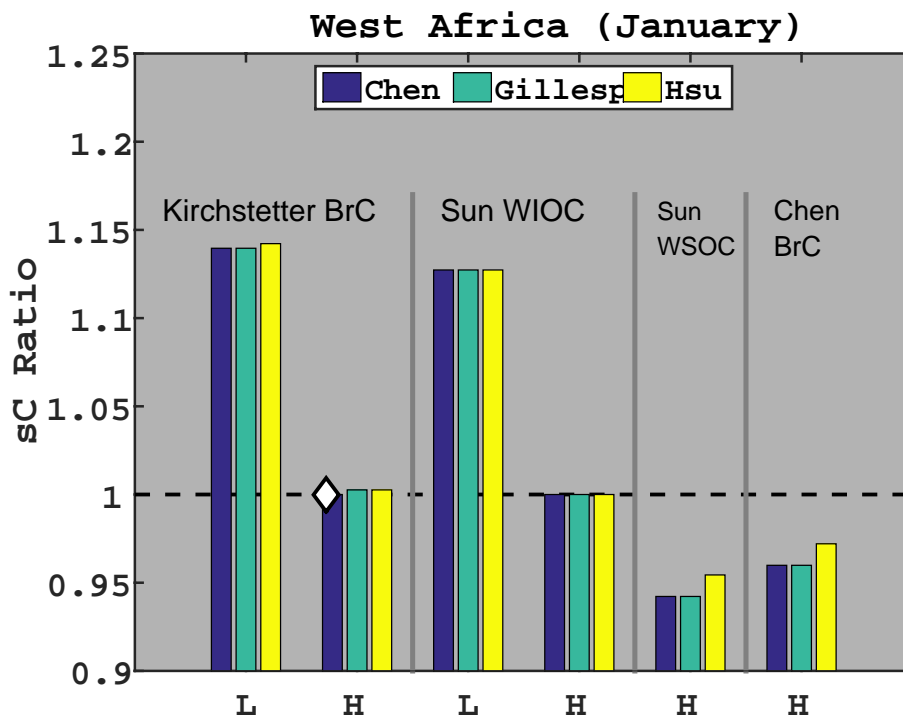


Figure 11. Relative bias associated with component refractive index uncertainty, utilizing 18 combinations of the refractive indices listed in Table 1. Each group of bars utilizes either the lowest (L) or highest (H) sC refractive index recommended by Bond and Bergstrom (2006). Groups of bars are also labeled according to the four BrC refractive index sources in Table 1; color code denotes hematite refractive index source. Baseline components are denoted by the diamond. Note that the sC bias associated with refractive index uncertainty is always less than 15%. See Table 1 for refractive index citations.

Title Page

Abstract Introduction

Conclusions References

Tables Figures

◀ ▶

◀ ▶

Back Close

Full Screen / Esc

Printer-friendly Version

Interactive Discussion



Remote sensing of different absorbing aerosol species

G. L. Schuster et al.

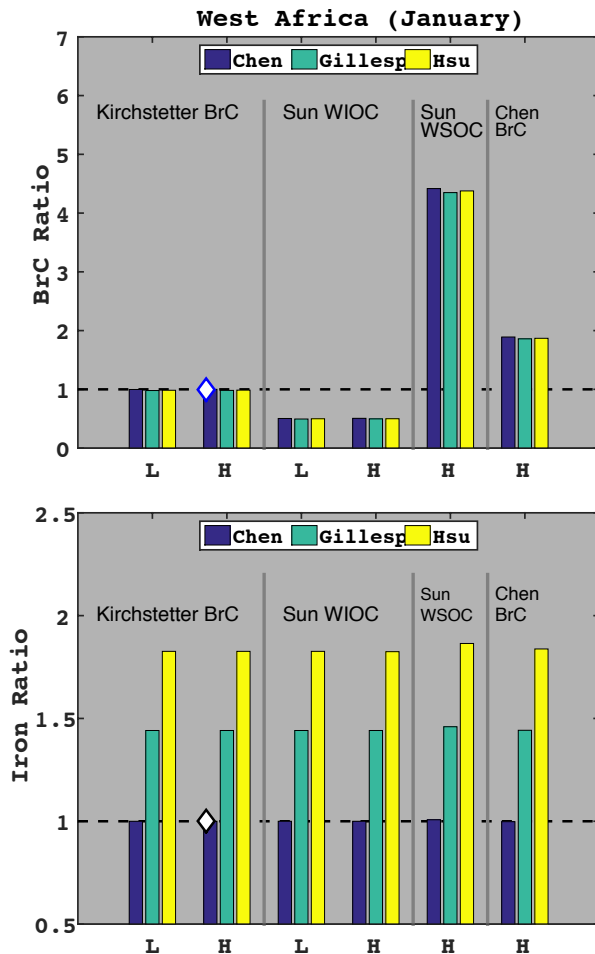


Figure 12. Same as Fig. 11, except y axis is BrC (top panel) and free iron (bottom panel) relative biases.

Title Page

Abstract Introduction

Conclusions References

Tables Figures

◀ ▶

◀ ▶

Back Close

Full Screen / Esc

Printer-friendly Version

Interactive Discussion



Remote sensing of different absorbing aerosol species

G. L. Schuster et al.

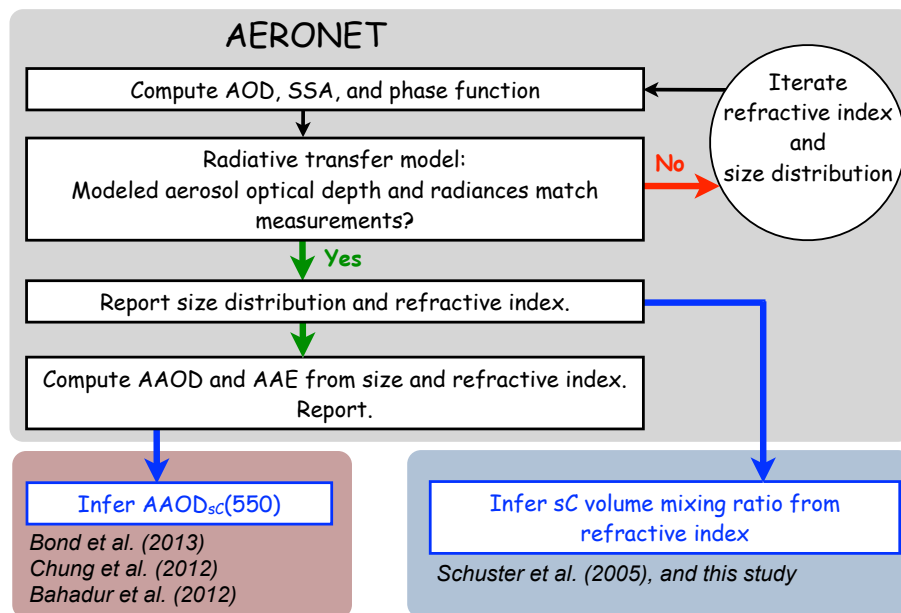


Figure 13. Retrieval schematic for AERONET (gray shading) and subsequent sC retrievals reported in the literature. The size distribution and the complex refractive index are the independent variables that are iterated in the AERONET product; AAOD and AAE are computed from these parameters. Maroon shading denotes various techniques that are based upon AAOD; blue shading denotes this study, which is based upon the refractive index.

Title Page	
Abstract	Introduction
Conclusions	References
Tables	Figures
◀	▶
◀	▶
Back	Close
Full Screen / Esc	
Printer-friendly Version	
Interactive Discussion	

